Journal of Applied Physics ARTICLE pubs.aip.org/aip/jap

Measurement of coating–substrate interface stiffness using a constructed ultrasonic echo phase derivative spectrum

Cite as: J. Appl. Phys. **135**, 145305 (2024); doi: 10.1063/5.0194969
Submitted: 29 December 2023 · Accepted: 26 March 2024 ·
Published Online: 12 April 2024

Tianzhi Qi,[1] Li Lin,[1] Zhiyuan Ma,[1,a)] Jiwei Yang,[1] and Yang Zhao[2,b)]

AFFILIATIONS

[1]NDT & E Laboratory, Dalian University of Technology, Dalian 116085, China
[2]School of Information Science and Engineering, Harbin Institute of Technology (Weihai) Weihai, Shandong 264209, China

[a)]**Author to whom correspondence should be addressed:** zhiyma@dlut.edu.cn
[b)]zhao.yang@hit.edu.cn

ABSTRACT

Measurement of coating–substrate interface stiffness can indirectly characterize interface bonding quality. This paper proposes a noval quantitative inversion coating–substrate interface stiffness method based on the multi-resonance frequencies of a constructed ultrasonic echo phase derivative spectrum (UEPDS). The theoretical relationship between UEPDS resonance frequencies and interface stiffness is derived. The detection frequency and high-sensitivity interface stiffness range are optimized based on the sensitivity analyzed. Numerical simulation and experiment are implemented on a 0.48 mm aluminum layer/carbon steel substrate specimen to prove the validity of the proposed ultrasonic method. The simulation results show that the maximal relative error between the inversion and the preset interface stiffnesses is reduced from 23% to 8% compared with the traditional ultrasonic reflection coefficient amplitude spectrum-based (URCAS-based) method. The experiment results indicate that the UEPDS-based inversion interface stiffnesses have the same trend as the nominal contact pressures between the coating–substrate interface.

I. INTRODUCTION

During the preparation process of radar absorption, sealing, thermal barrier, and other functional coatings, micro-defects such as cracks, pores, and inclusions are easily generated at the interface, significantly reducing the interface bonding quality and weakening key components' reliability and service life. Therefore, nondestructive characterization of the coating–substrate interface bonding quality during preparation and service is of great significance to ensure the yield and service reliability of the coating components.[1–3] Nondestructive testing methods of bonding quality such as laser speckle interferometry,[4,5] infrared thermal imaging,[6,7] radiographic testing,[8] and ultrasonic testing[9] have been applied to automobile manufacturing, aerospace, and other fields.

Many prior studies have demonstrated that the interfacial layers with different bonding qualities can be modeled as infinitely thin interfaces with different interface stiffnesses, and ultrasonic testing is sensitive to interface stress and displacement; it can be used to measure the interface stiffness.[10–12] Lavrentyev *et al.*[12] used 5 and 10 MHz probes to investigate the interface stiffnesses of 50 mm thick, S7 tool steel plate welded specimens with different bonding strengths and showed a good linear relationship between interface stiffness and interface bonding strength. Escobar-Ruiz[13,14] *et al.* proposed an interface stiffness detection method based on the echo phase. In his work, a 10 MHz probe was used to detect the interface stiffness of the 12.7 mm thick TC4 diffusion welding structure and performed a failure test on the low interface stiffness area. The results showed that there were textures and micro-unwelding defects in the low interface stiffness area of the diffusion weld interface. The above research studies have made great contributions to the non-destructive testing and evaluation of interface stiffness. However, these methods all need to extract independent interface echo or its characteristics, which

are only suitable for the detection of interface quality of the sample with a thick wall.

To detect the interface stiffness of thin-walled structures such as thin-walled welding, spraying, and adhesion bonding, the multiple interface reflection echoes and the surface reflection echo are usually overlapping, which is difficult to extract separately. The existing research usually analyzes the overlapping echo using the Fourier transform. The ultrasonic reflection coefficient amplitude spectrum (URCAS) or phase spectrum (URCPS) is constructed, and the characteristic parameters to characterize the interface stiffness such as resonant frequency and phase are extracted.[15–19] Lavrentyev *et al.*[15] proposed a URCAS-based interface stiffness characterization method. A constitutive relationship between URCAS resonance frequency and interface stiffness was derived. The interface reflection echoes of aluminum plate–0.5 mm aluminum layer–aluminum plate structure were collected by a 10 MHz probe under different load forces, and the URCAS resonance frequencies shifted to high frequency direction with the increase in interface stiffness. This method inverts the layer–substrate interface stiffness using a single resonance frequency. However, single resonance frequency sensitivity to interface stiffness is limited, and the inversion stiffnesses will be inaccurate while sensitivity is low. Qi *et al.*[17] analyzed the sensitivity of URCAS amplitude to interface stiffness at different frequencies. The high-sensitivity interface stiffness range and frequency range are defined, and an interface stiffness inversion method based on the URCAS amplitude in the high-sensitivity frequency range was proposed. In this work, the interface stiffnesses of 0.5 mm epoxy coating–aluminum substrate specimens were measured by a 7.5 MHz water immersion probe, and the bonding strengths of the corresponding coating specimens were measured by tensile test. The method can accurately quantify the coating–substrate structure interface stiffness and indirectly quantify the coating–substrate interface bonding strength. This work points out that the sensitivity of URCAS to interface stiffness is different in different frequency ranges and the inversion error increases significantly when sensitivity is low. However, coating microstructure, interface roughness, reference signal quality, and other factors can affect the amplitude of URCAS. In actual detection, especially when the material microstructure is complex, unknown amplitude influencing factors will affect the accuracy of the inversion interface stiffnesses. In addition to the URCAS method indicated above, Haldren *et al.*[18,19] proposed a URCPS-based interface stiffness characterization method and measured the interface stiffnesses of the glass–epoxy resin adhesive–glass structure adhesion specimens. The results show the feasibility of this method to characterize the bonding quality of the adhesion interface. Haldren *et al.* indicated that URCPS was affected by factors such as sound wave propagation time, sound attenuation, system phase, and signal initial phase, which could be summarized into the form of $af + b$. In his work, the *in situ* bottom echoes of the glass plate were pre-measured as reference signals before the preparation of the adhesive specimens, for eliminating the interference factors in the interface echoes such as wave propagation time, acoustic attenuation, system phase, and signal initial phase. This is difficult to achieve in practical engineering.

Based on the induction of interference factors in the interface echoes such as wave propagation time, acoustic attenuation, system phase, signal initial phase, and other factors on the ultrasonic echo phase indicated by Haldren *et al.*,[18,19] this paper proposes an inversion method for measuring the interface stiffness of coupling medium–coating–substrate three-medium two-interface structure based on a constructed ultrasonic echo phase derivative spectrum (UEPDS). The spring model is used to construct the UEPDS function when ultrasonic wave perpendicularly incident to the coupling medium–coating–substrate three-medium two-interface structure. The constitutive relationship between the resonance frequency of UEPDS and interface stiffness is derived, and a method for inverting the interface stiffness based on the resonance frequency of UEPDS is proposed. This method can effectively reduce the influence of the mentioned factors above. Based on the sensitivity analysis, the detection frequency is optimized. Aiming at the limited sensitivity of single resonance frequency inversion interface stiffness, an inversion method of constructing the least squares objective function based on multi-resonance frequencies of simulation/experiment and theory in the effective frequency band is proposed, and the genetic algorithm is used to get a precise inversion of interface stiffness.

II. PRINCIPLE

A. Ultrasonic wave interaction with three-medium two-interface structure

The propagation diagram of the ultrasonic wave perpendicularly incident into the coupling medium–coating–substrate three-medium two-interface structure is shown in Fig. 1.[20] The order interface 1 and 2 are coupling medium–coating interface and

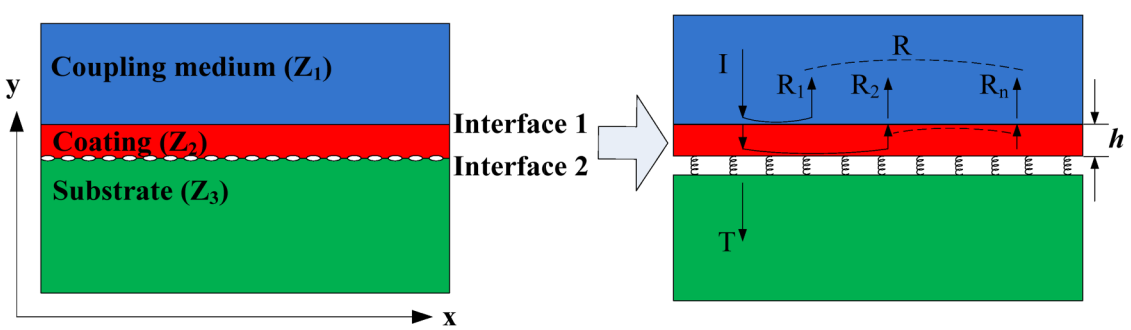

FIG. 1. Propagation diagram of an ultrasonic wave perpendicularly incident into coupling medium-coating-substrate three-medium two-interface structure.

coating–substrate interface, where interface 1 is a lubrication interface that can be equivalent to an ideal interface, and interface 2 is a random contact interface. In practical engineering, there are many micro-defects in the solid–solid bonding interface, such as pores, weak bondings, and disbondings, which are much smaller than the ultrasonic wavelength, causing the degradation of the interface bonding quality. Usually, the degraded bonding interface is defined as an imperfect interface. The mechanical properties and behavior of this kind of imperfect interface can be equivalent to a spring boundary condition using the spring model,[21] and its physical description is as shown in Eq. (1),

$$\sigma'_{yy} = K_n(u_y - u'_y),\ \sigma'_{yy} = \sigma_{yy}, \tag{1}$$

where the interface normal direction's stress and displacement are marked as σ_{yy} and u_y, respectively. Normal interface stiffness is marked as K_n. The interface can be equivalent to a completely disbonding state when K_n tends to 0. On the contrary, the interface can be equivalent to a perfect interface when K_n tends to ∞. Tattersall *et al.*[22] derived the interface reflection coefficient r_{ij} when the incident wave is perpendicular to the interface between medium j and medium i, based on spring boundary condition, as shown in Eq. (2),

$$r_{23} = \frac{(Z_3 - Z_2 + i(\omega/K_n)Z_2Z_3)}{(Z_2 + Z_3 - i(\omega/K_n)Z_2Z_3)}, \tag{2}$$

where ω is the angular frequency of the ultrasonic wave; Z_2 and Z_3 are the acoustic impedances of media 2 and 3, respectively; and their values are the product of sound velocity and density. The ultrasonic echoes reflected from the coupling medium–coating interface and coating–substrate interface are usually overlapping because of the thin thicknesses of coatings, and it is tough to distinguish the interface echo. Assuming that the amplitude of the incident acoustic wave is A, the phase of the system and the initial phase of the signal is φ_0, the frequency is f, the thickness of the coating is h, the wave number of the ultrasonic wave in the coating is k, and the propagation time of the ultrasonic wave in the coupling medium is t_0. The interface 1 is described as a perfect interface, and its reflection and transmission coefficients can be written as $r_{ij} = \frac{Z_j - Z_i}{Z_j + Z_i}$, $t_{ij} = \frac{2Z_i}{Z_j + Z_i}$. Then, the theoretical expressions of the incident wave I, the single reflected echo R_i, and the overlapping reflected echoes R of the coating in the detection model are shown in Eq. (3),

$$\begin{aligned} I &= A\exp(i\varphi_0) \\ R_1 &= Ar_{12}\exp(i(4\pi ft_0 + \varphi_0)) \\ R_2 &= At_{12}r_{23}t_{21}\exp(2ikh + 4\pi ft_0 + \varphi_0) \\ R_n &= At_{12}r_{23}^{n-1}r_{21}^{n-2}t_{21}\exp(2(n-1)ikh + 4\pi ft_0 + \varphi_0) \\ R &= R_1 + R_2 + \ldots + R_n = A\frac{(r_{12} + r_{23}\exp(2ikh))}{(1 + r_{12}r_{23}\exp(2ikh))}\exp(i(4\pi ft_0 + \varphi_0)). \end{aligned} \tag{3}$$

Substituting Eq. (2) into Eq. (3), the expression of the overlapping echoes phase $Phase_R$ is obtained, as shown in Eq. (4), where v_2 is the sound velocity of the coating,

$$\begin{aligned} &\mathrm{Phase}_R = \arctan\left(\frac{((1 - r_{12}^2)|r_{23}|\sin(\varphi))}{((1 + |r_{23}|^2)r_{12} + (1 + r_{12}^2)|r_{23}|\cos(\varphi))}\right) + (4\pi ft_0 + \phi_0) \\ &\text{and } \varphi = \arctan\frac{4\pi fK_nZ_3^2Z_2}{K_n^2(Z_3^2 - Z_2^2) - (2\pi fZ_3Z_2)} + \frac{4\pi fh}{v_2},\ |r_{23}| = \sqrt{\frac{(Z_3 - Z_2)^2K_n^2 + (2\pi fZ_3Z_2)^2}{(Z_3 + Z_2)^2K_n^2 + (2\pi fZ_3Z_2)^2}}. \end{aligned} \tag{4}$$

B. The relationship between UEPDS resonance frequency and interface stiffness

Equation (4) shows that Phase_R is not only affected by the phase of the multi-echo reflection coefficient but also by the initial phase of the system, time delay, and other factors.[18,19] This paper constructs UEPDS_R to decrease the influence of random phase caused by the initial phase and time delay of the signal by calculating the first derivative of frequency by Phase_R, UEPDS_R as shown in Eq. (5),

$$\begin{aligned} &\mathrm{UEPDS}_R = \frac{d\mathrm{Phase}_R}{df} \\ &\mathrm{UEPDS}_R = \frac{\left((1 - r_{12}^2)r_{12}\left(\sqrt{\left((1 + |r_{23}|^2)|r_{23}|\frac{d\varphi}{df}\right)^2 + \left((1 - |r_{23}|^2)\frac{d|r_{23}|}{df}\right)^2}\cos\left(\varphi + \arctan\frac{(1 - |r_{23}|^2)d|r_{23}|}{(1 + |r_{23}|^2)|r_{23}|d\varphi}\right)\right)\right) + (1 - r_{12}^2)(1 + r_{12}^2)|r_{23}|^2\frac{d\varphi}{df}}{(r_{12}^2 + (1 - r_{12}^2)^2|r_{23}|^2 + 2r_{12}(1 + r_{12}^2)|r_{23}|\cos(\varphi) + 4r_{12}^2|r_{23}|^2\cos^2(\varphi))}, \end{aligned} \tag{5}$$

where

$$\frac{d|r_{23}|}{df} = \frac{16fZ_3Z_2K_n^2(\pi Z_3Z_2)^2}{((Z_3+Z_2)^2K_n^2+(2\pi fZ_3Z_2)^2)\left(\sqrt{((Z_3-Z_2)^2K_n^2+(2\pi fZ_3Z_2)^2)((Z_3+Z_2)^2K_n^2+(2\pi fZ_3Z_2)^2)}\right)},$$

$$\frac{d\varphi}{df} = \frac{4\pi h}{v_2} + \frac{d\varphi_R}{df},$$

$$\frac{d\varphi_R}{df} = \frac{4\pi K_n Z_3^2 Z_2(K_n^2(Z_3^2-Z_2^2)+f(2\pi Z_3Z_2)^2)}{(4\pi fK_nZ_3^2Z_2)^2+(K_n^2(Z_3^2-Z_2^2)-(2\pi fZ_3Z_2)^2)^2},$$

where

$$\frac{d\varphi_R}{df} << \frac{4\pi h}{v_2}, \qquad \frac{d|r_{23}|}{df} << \frac{4\pi h}{v_2}, \text{ so}$$

$$\cos\left(\varphi + \arctan\frac{(1-|r_{23}|^2)d|r_{23}|}{(1+|r_{23}|^2)|r_{23}|d\varphi}\right) \approx \cos(\varphi).$$

Therefore, Eq. (5) can be simplified to Eq. (6),

$$\mathrm{UEPDS}_R = \frac{\left((1-r_{12}^2)r_{12}\sqrt{((1+|r_{23}|^2)|r_{23}|d\varphi)^2+((1-|r_{23}|^2)d|r_{23}|)^2}\cos(\varphi)\right)+(1-r_{12}^2)(1+r_{12}^2)|r_{23}|^2d\varphi}{\left(\left(2r_{12}|r_{23}|\cos(\varphi)+\frac{1}{2}(1+r_{12}^2)\right)^2-\frac{1}{4}(1+r_{12}^2)^2+r_{12}^2+(1-r_{12}^2)^2|r_{23}|^2\right)df}. \tag{6}$$

According to Eq. (6), when $\varphi = (2k+1)\pi$, UEPDS is at extreme value, the frequencies corresponding to extreme value is defined as the UEPDS resonance frequencies. Introducing the following non-dimensional parameters:

$$\zeta = (1-r_{12}^2)(1+r_{12}^2)|r_{23}|^2d\varphi,\ \psi = (1-r_{12}^2)r_{12}\sqrt{((1+|r_{23}|^2)|r_{23}|d\varphi)^2+((1-|r_{23}|^2)d|r_{23}|)^2}.$$

So UEPDS is maximum or minimum at the resonance frequencies depending on the values of the non-dimensional parameters ζ and ψ. If $\zeta > \psi$, UEPDS is minimum in the resonance frequencies; if $\zeta < \psi$, UEPDS is maximum in the resonance frequencies. According to Eqs. (4) and (6), the expression of resonance frequency can be written as Eq. (7),

$$f_{(2n+1)} = \frac{\left((2n+1)\pi - \arctan\frac{4\pi fK_nZ_3^2Z_2}{K_n^2(Z_3^2-Z_2^2)-(2\pi fZ_3Z_2)^2}\right)v_2}{4\pi h}. \tag{7}$$

It can be seen that the UEPDS resonance frequencies are significantly related to the interface stiffness K_n. The coating thickness h in Eq. (7) can be measured in advance through the interval of two resonance frequencies, as shown in Eq. (8). It is feasible to invert the interface stiffness by UEPDS resonance frequencies,

$$h \approx \frac{v}{2\Delta f}, \quad \Delta f = f_{2(n+1)+1} - f_{2n+1}. \tag{8}$$

C. Sensitivity analysis

According to the analysis of Eq. (2), the ultrasonic wave with a specific frequency is only sensitive to the stiffness in a specific range. The function ω/K_n is the coupling result of interface stiffness and detection frequency. When ω/K_n tends to ∞, the interface is equivalent to the complete debonding state, and the reflection coefficient is $R \approx 1$. When ω/K_n tends to 0, the interface is equivalent to the perfect interface. The coupling medium–coating–substrate structure overlapping echoes reflection coefficient has multiple UEPDS resonance frequencies from low frequency to high frequency. Different resonance frequencies have different detection sensitivities to interface stiffness. Lavrentyev *et al.*[23] considered that sensitivity greatly influences the test results, and low sensitivity will significantly reduce the posedness of the inversion results. Therefore, analyzing the sensitivity of different resonance frequencies to interface stiffness, and then optimizing the detection frequency, can effectively improve the well-posedness of the detection results.[24,25] The traditional sensitivity analysis is normalized to obtain the relative change of UEPDS resonance frequencies f_n with the change of interface stiffness K_n. As the order of the resonance frequency f_n increases, the absolute changing value of the high-order resonance frequency increases with the change in the interface stiffness, but the relative changing value decreases. Therefore, the sensitivity discussed in this work is the absolute changing value of resonance frequency f_n

TABLE I. Acoustic parameters of plexiglass–aluminum coating–carbon steel substrate structure.

Material	Sound velocity ($m\,s^{-1}$)	Density ($kg\,m^{-3}$)	Acoustic impedance ($kg\,m^{-2}\,s^{-1}$)	Thickness (μm)
Plexiglass	2331	1073	2.50×10^{6}	9980
Aluminum layer	6311	2689	16.97×10^{6}	480
Carbon steel substrate	5863	7821	45.86×10^{6}	9970

with the change in interface stiffness K_n, as shown in Eq. (9),

$$S_{f,K_n}=\frac{K_n\partial f_n}{|\partial K_n|}. \tag{9}$$

In order to correspond to the numerical simulation and experiment, this section takes the plexiglass–aluminum coating–carbon steel substrate structure as an example to introduce the whole process of sensitivity analysis. The acoustic parameters of each medium are shown in Table I. Figure 2(a) gives two resonance frequencies f_3 and f_5 of plexiglass–aluminum coating–carbon steel substrate structure with different interface stiffness. Figure 2(b) gives the sensitivities of f_3 and f_5 to the interface stiffness K_n. Considering that the frequency resolution after FFT transform in this work is 0.01 MHz, to ensure that the resonance frequency offset after stiffness change exceeds two FFT data points, this paper calibrates the sensitivity $S_{f,K}>0.02$ MHz as the demarcation criterion of the high-sensitivity range. In practical engineering, the microstructure and attenuation of the material to be tested will also affect the resonance frequency. Low sensitivity will introduce large measurement errors. Based on the demarcation criterion, the lower limit stiffness K_L and the upper limit stiffness K_U of the high-sensitivity range are determined as 1.5×10^{14} and $9.6\times10^{15}\,N\,m^{-3}$. With the order of resonance frequency increasing, the high-sensitivity interface stiffness range shifts to the high stiffness direction.

D. Inversion method

Based on the theoretical derivation in Sec. II B, resonance frequency f_n is an implicit function of stiffness K_n. The stiffness K_n needs to be calculated by inversion, and resonance frequency can be written as $f_n(Z, f, h, K_n, \ldots)$. According to Fig. 2(b), due to the limited sensitivity of a single resonance frequency to interface stiffness, the high-sensitivity stiffness range of different resonance frequencies is different. An inversion method based on multi-resonance frequencies is proposed. This method can combine the high-sensitivity stiffness range of different resonance frequencies, thereby expanding the high-sensitivity stiffness range. High sensitivity solves the problem of large inversion error caused by the low sensitivity of partial stiffness, and the stability of inversion results is further improved. The objective function fitness (K_n) is constructed by the experimental and theoretical resonance frequencies as shown in Eq. (10),

$$\begin{aligned} F(K_n)&=\sum_{n=1}^{N}\left(f_n^{\exp}(Z,f,h,K_n,\ldots)-f_n^{\text{the}}(Z,f,h,K_n,\ldots)\right)^2\\ \text{fitness}\,(K_n)&=\min\{F(K_n)\}, \end{aligned} \tag{10}$$

where N is the number of resonance frequencies in the effective frequency band and n is the order of resonance frequencies. After constructing the objective function, the minimum objective function is obtained based on the genetic algorithm to achieve accurate inversion of stiffness.

III. SIMULATION

A. Simulation model

In this section, a series of numerical simulation coating models were carried out using COMSOL Multiphysics to verify the validity of

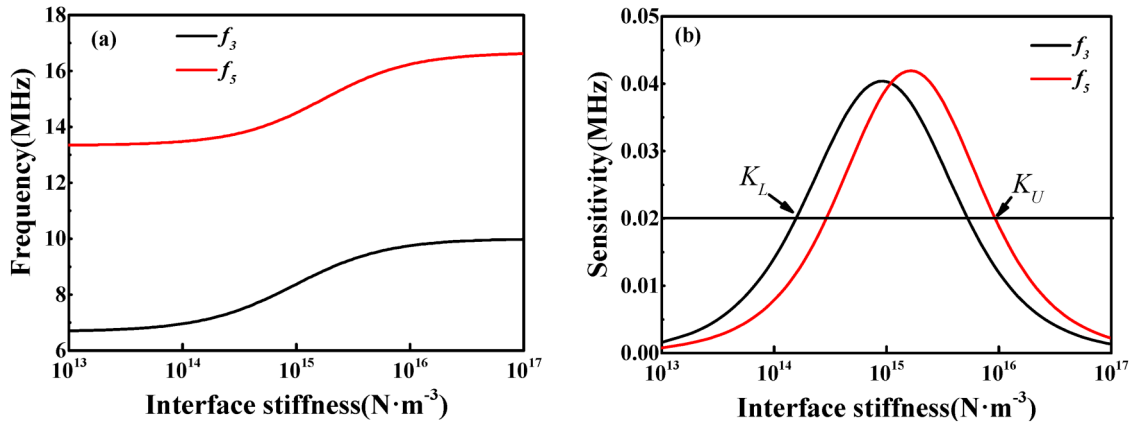

FIG. 2. Theoretical sensitivity analysis of different resonance frequencies to interface stiffness: (a) resonance frequencies with different interface stiffness; (b) sensitivities of resonance frequency to interface stiffness.

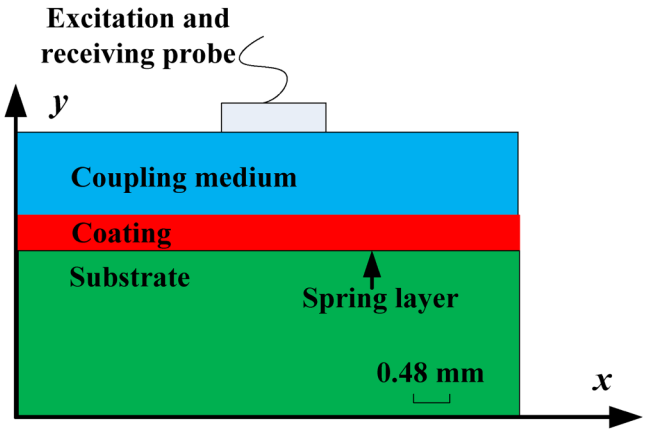

FIG. 3. The schematic diagram of the numerical simulation model.

the proposed UEPDS-based method and to avoid the difficulty of preparing a series of coating specimens with specific interface stiffness in practical engineering. Figure 3 shows the numerical simulation model schematic diagram; the thickness of coating and substrate are 0.48 and 3 mm, respectively. The symmetry boundaries were set at the left and right boundaries to ensure no transformed waves. The low-reflecting boundary was set at the bottom boundary, and the excitation and receiving probe for the ultrasonic source were loaded at the top boundary. A Gaussian sine pulse function was set as the excitation source time function, as shown in Eq. (11), where A is the ultrasound amplitude, t_P is the pulse duration, f is the ultrasound center frequency, and Q is the bandwidth coefficient. According to the CFL (Courant–Friedrichs–Lewy) criterion,[26] the grid size is required to be less than 1/20 of the smallest wavelength, and the time step is also required to be less than 1/20 of the corresponding dominant frequency. The coupling medium–coating interface is set as an ideal interface, and the layer–substrate interface is set as a spring boundary condition to simulate the random contact state based on the spring model. Each medium acoustic parameter is given in Table I,

$$g(t) = \begin{cases} A\exp\left(-\dfrac{(t-t_P/2)^2}{Q^2}\right)\sin(2\pi ft), & 0 < t \le t_0 \\ 0, & \text{others} \end{cases}. \quad (11)$$

The sensitivity of the two resonance frequencies of f_3 and f_5 to the interface stiffness was discussed in Sec. II. Considering the high-sensitivity interface stiffness ranges, the nominal 7.5 MHz center frequency probe is selected as the simulated excitation source. The time domain and frequency domain signals of the excitation source are shown in Fig. 4.

In this paper, 14 group simulation models with interface stiffness of 3×10^{13}, 5×10^{13}, 7×10^{13}, 1×10^{14}, 3×10^{14}, 5×10^{14}, 7×10^{14}, 1×10^{15}, 3×10^{15}, 5×10^{15}, 7×10^{15}, 1×10^{16}, 3×10^{16}, and 5×10^{16} N m^{-3} were established.

B. Simulation results

The simulated echoes of four numerical simulation models with different interface stiffnesses are shown in Fig. 5(a). The interface echo amplitudes decrease significantly with the stiffness increases. Figures 5(b) and 5(c) show the URCASs and UEPDSs, and the resonance frequencies f_3 extracted based on URCAS and UEPDS are shown in Fig. 5(d). Obviously, the resonance frequencies extracted based on UEPDS are closer to the theoretical values. In the high-sensitivity interface stiffness range, the maximal relative error of the inversion stiffnesses using the traditional URCAS-based method is 23%, while that using the UEPDS-based method is 14%. As the interface stiffness increases, the resonance frequency deviation between URCAS and UEPDS gradually decreases. When the stiffness exceeds 5×10^{15} N m^{-3}, there is almost no deviation.

After extracting the resonance frequencies, constructing the objective function, the minimum objective function is constructed based on the genetic algorithm to achieve accurate inversion of

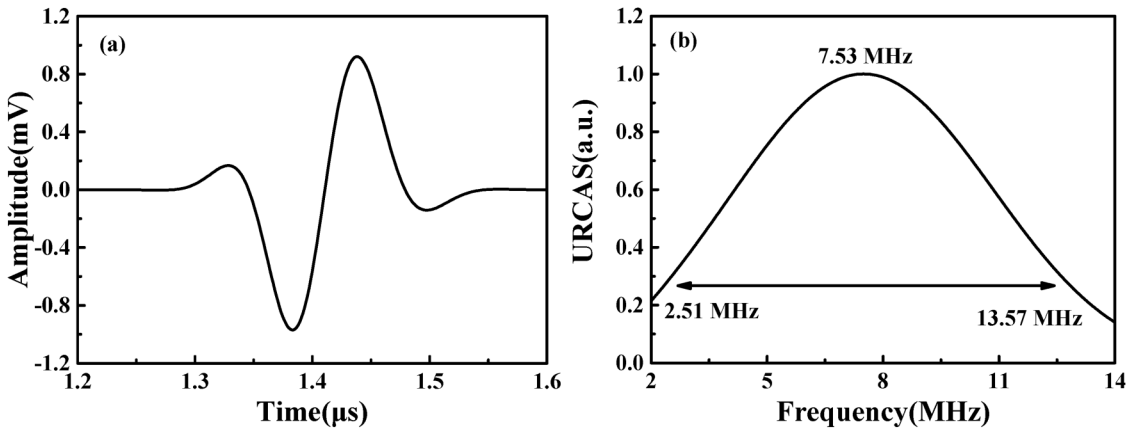

FIG. 4. Simulated excitation source: (a) time domain signal; (b) frequency spectrum.

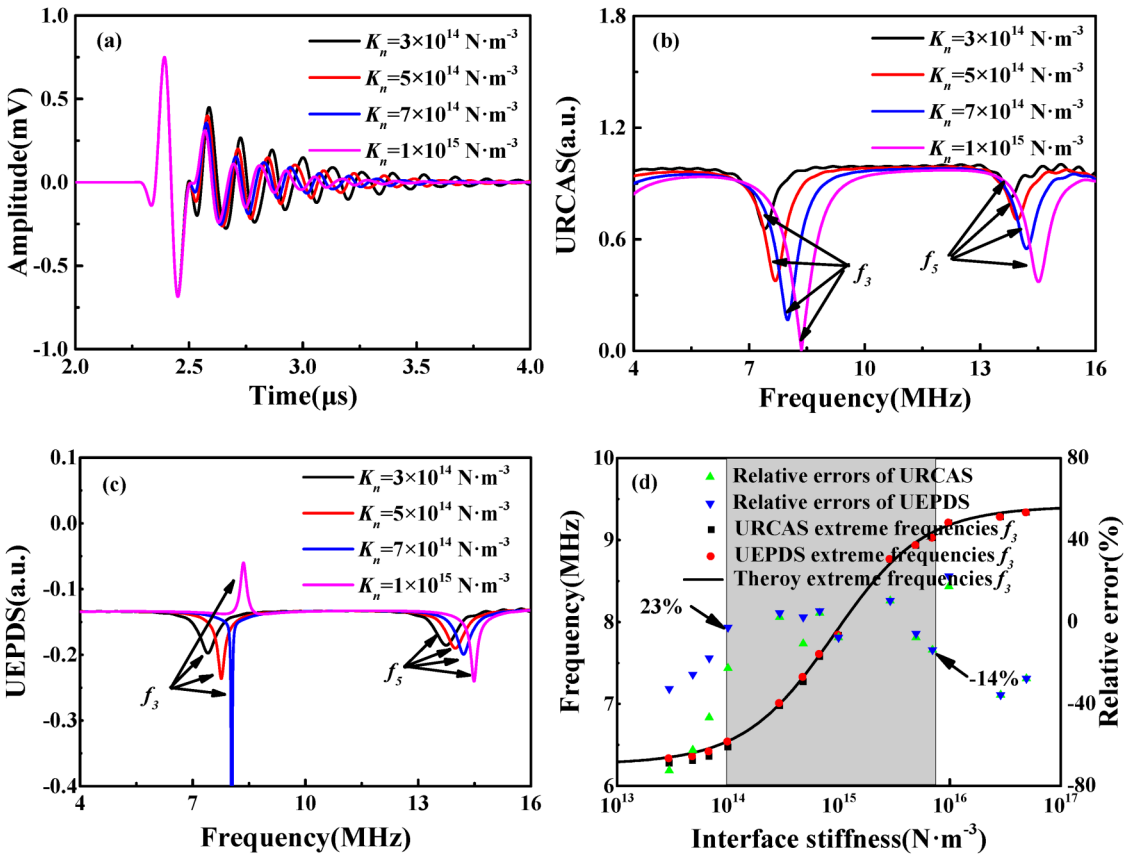

FIG. 5. Comparison of URCAS-based and UEPDS-based interface stiffness inversion methods: (a) simulating echoes; (b) URCASs; (c) UEPDSs; (d) relative errors of interface stiffness inversion based on URCAS and UEPDS.

stiffness. In the inversion process, based on the high-sensitivity interface stiffness range, the inversion stiffness range is set to 10^{13}–10^{17} N m^{-3}. Each interval between 10^n and 10^{n+1} N m^{-3} is divided into 100 intervals. The population size of the genetic algorithm is set to 400, the number of iterations is 600, the crossover probability is 0.5, and the mutation probability is 0.1.

Figure 6 shows the inversed interface stiffnesses based on the extracted UEPDS resonance frequencies. Figure 6(a) shows that, with different interface stiffnesses, the extracted UEPDS resonance frequencies have a good agreement with the theoretical resonance frequencies. Figure 6(b) shows a good agreement between the inversion stiffnesses and the preset stiffnesses. Figure 6(c) shows the relative error between the inversion interface stiffness and the preset interface stiffness based on the single-resonance frequency inversion method and the multi-resonance frequencies inversion method. The maximal inversion relative error is 8% based on multi-resonance frequencies in the high-sensitivity stiffness range. Outside the high-sensitivity stiffness range, the relative errors are significantly increasing, and exceeding 30%, which is difficult to accurately quantify the interface stiffness. In this method, the high-sensitivity stiffness range is extended to 1×10^{14}–1×10^{16} N m^{-3}, while the high-sensitivity stiffness range of the single-resonance frequency inversion method based on f_3 or f_5 is only 1.4×10^{14}–5.5×10^{15} N m^{-3} or 3.2×10^{14}–9.5×10^{15} N m^{-3}. The proposed UEPDS-based method combined with the proposed multi-resonance frequency inversion method can improve the inversion accuracy and expand the inversion stiffness range. It shows good detection stability.

IV. EXPERIMENT

A. Specimens and testing system

Figure 7 shows the diagram of the experimental system. The contacted specimen consists of a 76 mm diameter and 9.8 mm thick cylindrical plexiglass (top), a 76 mm diameter and 0.48 mm thick cylindrical aluminum layer (mid-layer), and a 30 mm diameter and 9.7 mm thick cylindrical carbon steel substrate (bottom). The surfaces of the three components above were processed in parallel. The contact surfaces were polished with #1000 sandpaper. In the plexiglass–aluminum layer interface, some coupling liquid was

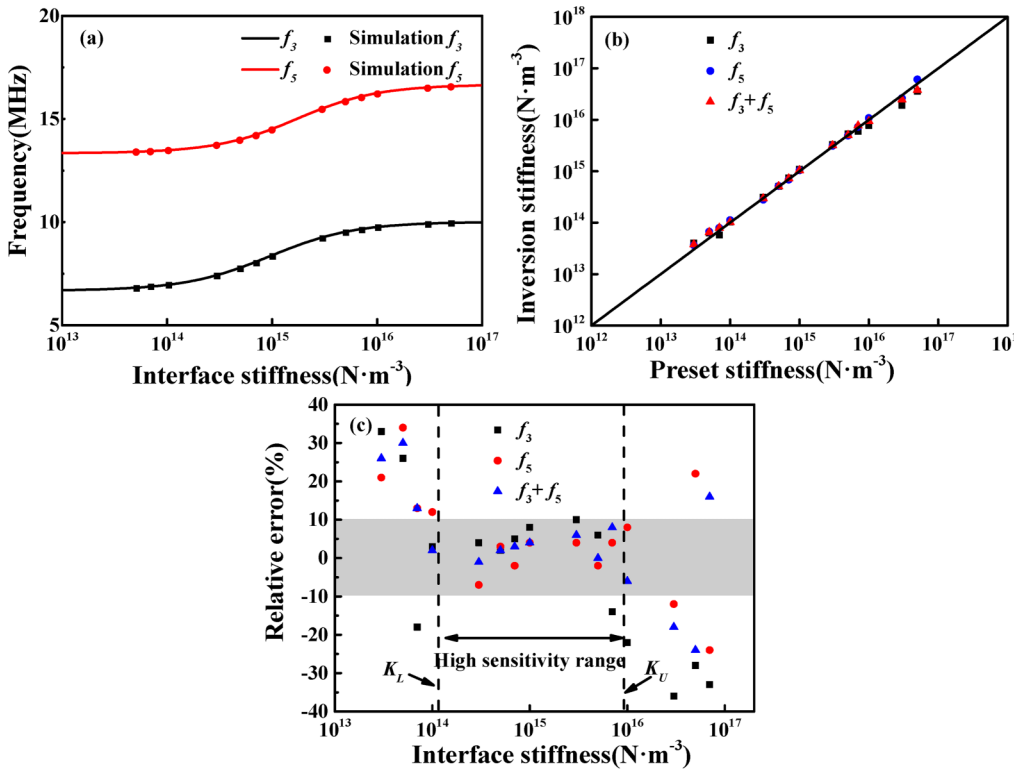

FIG. 6. Interface stiffness inversion results: (a) comparison of measured resonance frequencies and theoretical resonance frequencies; (b) inversion interface stiffnesses; (c) inversion relative errors.

added to the 8 mm diameter area that coincides with the center of the circle to ensure that the interface is wet during the detection, and the remaining area was bonded with epoxy resin that is cured under 30 N constant load force to ensure that the interface coupling state does not change during loading. The aluminum layer–carbon steel substrate interface was a direct contact interface. The specimen and fixture were assembled and placed on a universal testing machine. The interface stiffness of the aluminum layer–carbon steel substrate interface is changed by changing the load. A longitudinal wave transducer with a center frequency of 7.5 MHz was placed on the top of the plexiglass wedge. The top of the transducer was fixed with a spring to ensure the stability of the coupling state during the whole experiment. Subsequently, a TEK DPO4032 digital oscilloscope was used to amplify, digitize, average, and collect the ultrasonic reflection signals.

B. Experimental results

The step of load lifting was set to 1 kN, which can be converted to about 1.4 MPa pressure, and the ultrasonic data were collected once every step. The echoes with different loads are shown in Fig. 8(a). As the load increases, the echo amplitude of the aluminum layer–carbon steel substrate interface decreases significantly. Figure 8(b) shows the UEPDSs$_{exp}$. The resonance frequencies shift to the high frequency direction with the increase in load.

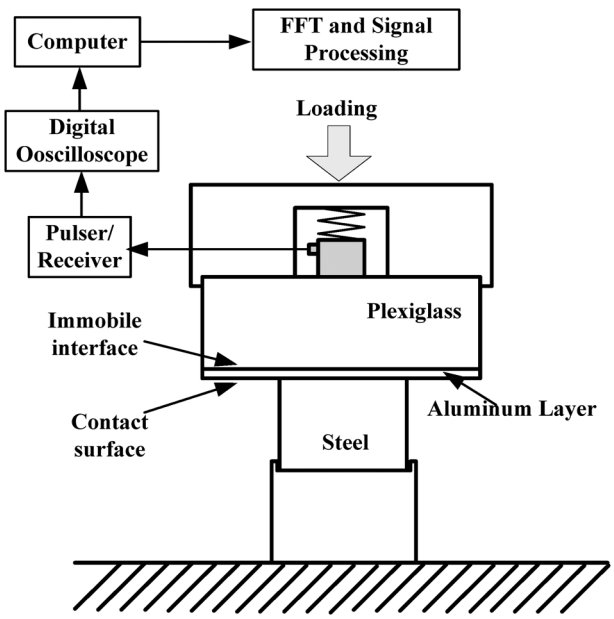

FIG. 7. Diagram of the experimental system.

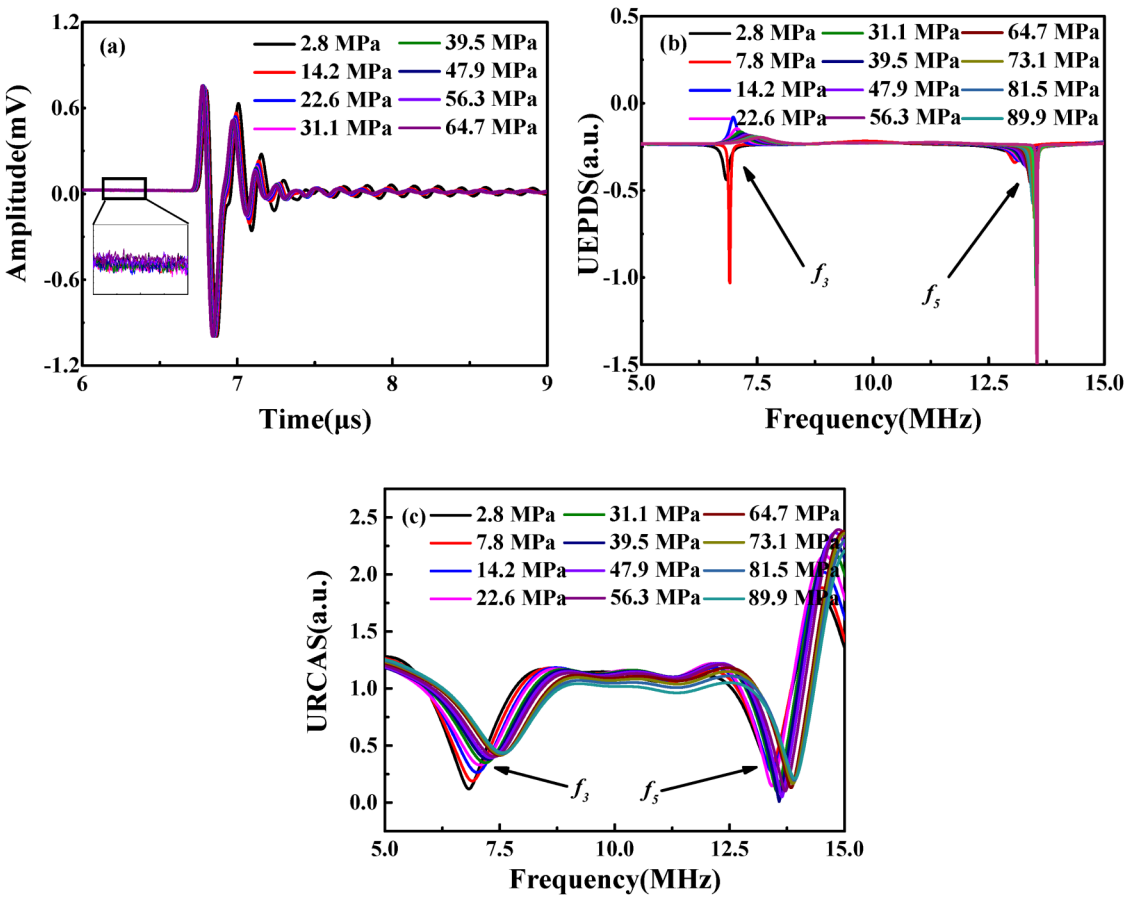

FIG. 8. Ultrasonic echo signals of plexiglass–aluminum layer–carbon steel substrate under different pressures: (a) echo signals; (b) UEPDSs; (c) URCASs.

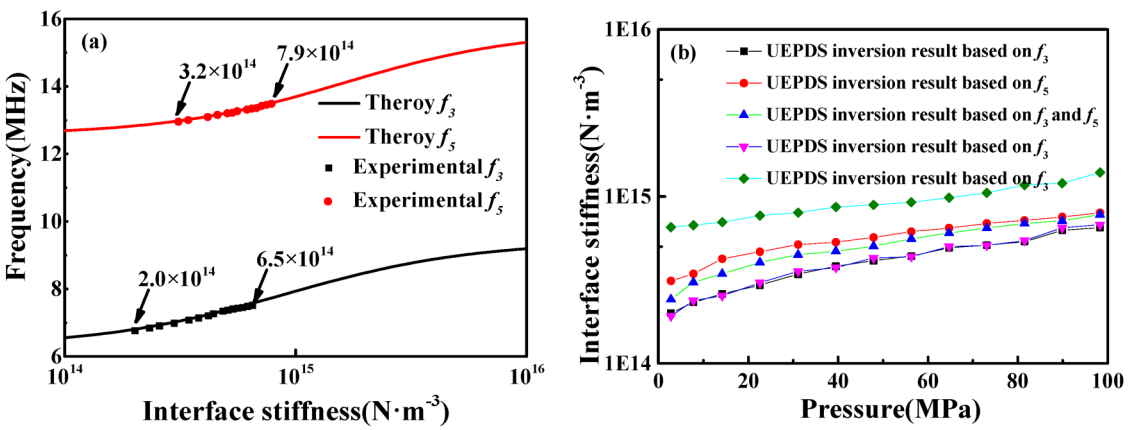

FIG. 9. Inversion results: (a) comparison of experimental single-resonance frequency f_3 or f_5 with theoretical resonance frequency; (b) the inversion stiffnesses of the URCAS-based method and UEPDS-based method.

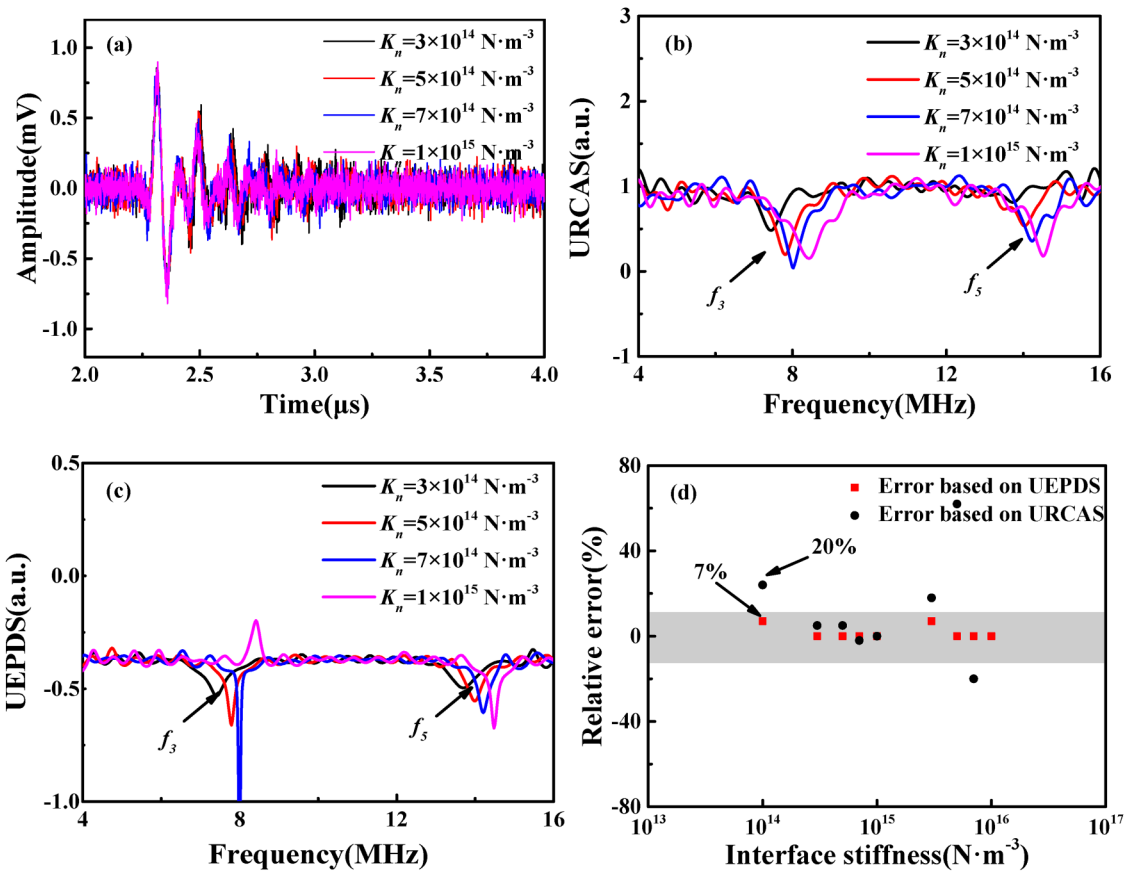

FIG. 10. Simulation signal and inversion results under noise: (a) echoes; (b) URCASs; (c) UEPDSs; (d) inversion relative errors.

To compare with the inversion results of the URCAS-based method proposed by Lavrentyev *et al.*,[15] the $URCASs_{exp}$ are obtained by performing FFT transform on the echoes as shown in Fig. 8(c). The resonance frequencies can be clearly extracted, which is in good agreement with the UEPDS results.

Figure 9 shows the inversion interface stiffnesses. Figure 9(a) shows the inversion stiffnesses based on single-resonance frequency f_3 or f_5, and the inversion stiffnesses by the two single resonance frequencies are significantly different. When the pressure is 2.8 MPa, the inversion stiffness based on f_3 is 2×10^{14} N m^{-3}, while the inversion stiffness based on f_5 is 3.2×10^{14} N m^{-3}, and the relative error between the two is 60%. When the pressure is 89.9 MPa, the inversion stiffness based on f_3 is 6.5×10^{14} N m^{-3}, while the inversion stiffness based on f_5 is 7.9×10^{14} N m^{-3}, the relative error is still as high as 22%, and the absolute error is 1.4×10^{14} N m^{-3}. Figure 9(b) shows the inversion results of the URCAS-based method and the UEPDS-based method. Based on resonance frequency f_3, the results of the URCAS-based method and the UEPDS-based method are in good agreement. But based on resonance frequency f_5, the inversion results of the URCAS-based method are significantly inaccurate. There is a certain amplitude of noise in the experimental signal as shown in Fig. 8(a). The amplitude of the noise is fixed in the spectrum and has a great influence on the low amplitude frequency region of the signals. This may be the reason that causes a significant inaccuracy result of the URCAS-based method resonance frequency f_5. Figure 9(b) also shows the inversion interface stiffnesses based on multi-resonance frequencies. The results are lower than inversion stiffnesses by f_5 and higher than inversion stiffnesses by f_3, and the three inversion results have similar trends.

V. DISCUSSION

Numerical simulation and experimental results demonstrate the feasibility of the proposed interface stiffness inversion method based on UEPDS resonance frequency. Compared with the traditional URCAS-based method, this method is more accurate in detection interface stiffness and does not need a reference signal. The experimental and simulation results also show that the inversion method based on multi-resonance frequencies has higher stability and accuracy than the inversion method based on a single-resonance frequency.

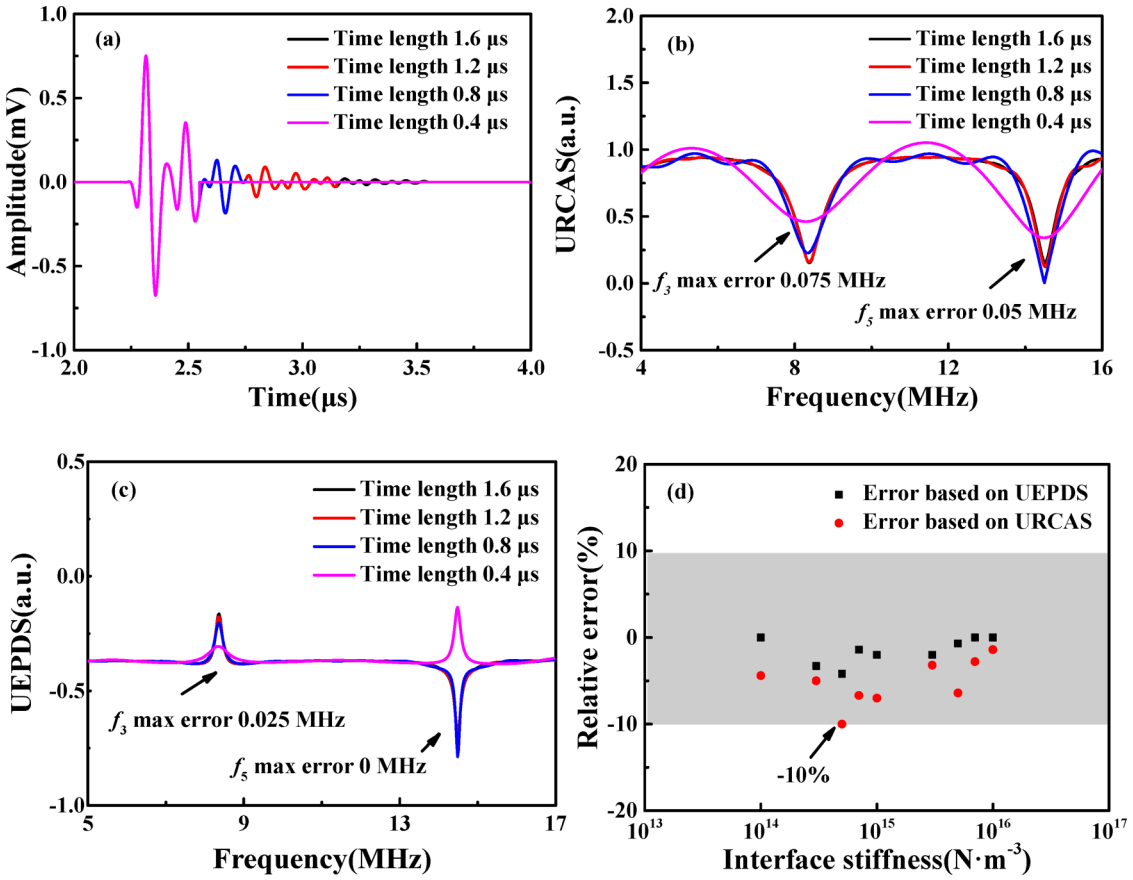

FIG. 11. Echoes and inversion results of different interception positions: (a) echoes; (b) URCASs; (c) UEPDSs; (d) inversion relative errors.

Testing system and structural noise will affect the experimental signal, thus affecting the accuracy of the detection results. The anti-noise ability of the detection method is very important in actual detection. Based on the simulation original signals of this paper, white noise with −12 dB peak intensity was added. Figure 10(a) shows the simulation echoes, which are seriously affected by the added noise. Figures 10(b) and 10(c) show the URCAS and UEPDS, respectively. The amplitudes of URCASs are obviously affected by noise, and the resonance frequencies f_3 and f_5 can only be extracted partially. UEPDSs are relatively less affected by noise, and the resonance frequencies f_3 and f_5 can be extracted clearly. Figure 10(d) shows the relative error of the two methods' inversion results between with noise and without noise conditions. The traditional URCAS-based method further produced a large error under the influence of noise, with a maximum of more than 20%, while the UEPDS-based method produced a smaller error, with a maximum of 7%. The UEPDS-based interface stiffness inversion method reflects stronger robustness.

In actual detection, the thicknesses of tested specimen substrates may be thin, and the echoes of the substrate bottom may interfere with the interception of the interface multi-echoes. Figure 11 discusses the effects of URCAS and UEPDS based on different intercept length time-domain echoes on resonance frequency extraction and interface stiffness inversion. Figure 11(a) shows the simulated echoes with different intercept lengths when the interface stiffness is 1×10^{15} N m^{-3}. Figures 11(b) and 11(c) show the corresponding URCASs and UEPDSs, respectively. Compared with the intercepted position length of 1.6 μs, the resonance frequencies f_3 of URCAS and UEPDS are shifted when the intercepted position length is 0.4 μs. The maximal shift of URCAS resonance frequencies f_3 is 0.075 MHz, while the UEPDS resonance frequencies' maximum shift is only 0.025 MHz. Figure 11(d) shows the relative error of the inversion stiffness when the echo interception time is 0.4 compared to 1.6 μs based on URCAS and UEPDS. The maximal error of the URCAS-based method due to the different echo interception positions is 10%, while the maximal error of the UEPDS-based method is 4.2%.

The results show that the proposed UEPDS-based method does not need a reference signal compared with the URCAS-based method. At the same time, it has the advantages of high accuracy, high stability, strong robustness, and less influence by signal interception position. However, the proposed method has the above-

mentioned advantages, there are still some limitations. First of all, the proposed method is more suitable for detecting homogeneous coatings. When detecting nonhomogeneous coatings with complex structures, high-frequency scattering will seriously affect UEPDS, and the extraction of resonant frequency needs to be corrected or compensated according to the material characteristics. For the selection of excitation source frequency bandwidth or center frequency, the narrow-band excitation source is suitable for the case of large coating thickness and low sound velocity, and the corresponding resonance frequency interval is small. For the detection of coating with a small thickness and high sound velocity, a wide-band excitation source and a matching detection system are required.

VI. CONCLUSION

(1) The constitutive relationship between the UEPDS resonance frequency and the interface stiffness of coupling medium–coating–substrate three-layer double-interface structure is derived based on the spring model. An interface stiffness inversion method based on the UEPDS resonance frequency is proposed. Compared with the method based on the URCAS minimum frequency, the proposed method does not need a reference signal and has the advantages of strong accuracy, strong robustness, and little influence by signal interception position.
(2) Based on the sensitivity analysis, the high-sensitivity interface stiffness ranges of different resonance frequencies to interface stiffness are determined. An inversion method based on multi-resonance frequencies is proposed. Compared with the single-resonance frequency inversion method, this method has higher stability and a larger high-sensitivity interface stiffness inversion range.
(3) The simulation results show that in the determined high-sensitivity stiffness range, the maximal relative error between the inversion and the preset stiffness is reduced from 23% to 14% compared with the traditional URCAS-based method. The maximal relative error through multi-resonance frequencies is further reduced from 14% to 8% compared with using the single-resonance frequency method. The high-sensitivity stiffness range is expanded from 1.5×10^{14}–9.6×10^{15} to 1×10^{14}–3×10^{16} N m^{-3}, and the high cut-off stiffness is expanded by more than 300%.
(4) The experimental results show the feasibility of the UEPDS-based inversion method in actual detection. The inversion stiffnesses through multi-resonance frequencies and single-resonance frequencies have similar trends. The UEPDS-based method shows effective interface stiffness quantitative ability and is expected to be used to characterize the bonding quality of the coating–substrate interface.

ACKNOWLEDGMENTS

This work was supported by the National Natural Science Foundation of China (NNSFC) (Grant Nos. U22B2068, 52175496, and 52075078).

AUTHOR DECLARATIONS

Conflict of Interest

The authors have no conflicts to disclose.

Author Contributions

Tianzhi Qi: Data curation (lead); Formal analysis (lead); Investigation (lead); Methodology (lead); Writing – original draft (lead). **Li Lin:** Funding acquisition (lead); Project administration (equal); Resources (lead); Writing – review & editing (equal). **Zhiyuan Ma:** Formal analysis (equal); Funding acquisition (equal); Methodology (equal); Resources (equal); Writing – review & editing (equal). **Jiwei Yang:** Data curation (supporting); Writing – review & editing (supporting). **Yang Zhao:** Investigation (equal); Project administration (equal).

DATA AVAILABILITY

The data that support the findings of this study are available from the corresponding author upon reasonable request.

REFERENCES

[1]Z. Y. Ma, W. Zhang, P. C. Du *et al.*, "Nondestructive measurement of elastic modulus for thermally sprayed WC-Ni coatings based on acoustic wave mode conversion by small angle incidence," NDT E Int. **94**(3), 38–46 (2018).
[2]A. Vencl, S. Arostegui, G. Favaro *et al.*, "Evaluation of adhesion/cohesion bond strength of the thick plasma spray coatings by scratch testing on coatings cross-sections," Tribol. Int. **44**(11), 1281–1288 (2011).
[3]L. J. Gu, X. Z. Fan, Y. Zhao *et al.*, "Influence of ceramic thickness on residual stress and bonding strength for plasma sprayed duplex thermal barrier coating on aluminum alloy," Surf. Coat. Technol. **206**(21), 4403–4410 (2012).
[4]G. Kim, S. Hong, K. Y. Jhang *et al.*, "NDE of low-velocity impact damages in composite laminates using ESPI, digital shearography and ultrasound C-scan techniques," Int. J. Precis. Eng. Manuf. **13**(6), 869–876 (2012).
[5]M. Ducousso, S. Bardy, Y. Rouchausse *et al.*, "Quantitative evaluation of the mechanical strength of titanium/composite bonding using laser-generated shock waves," Appl. Phys. Lett. **11**(112), 1–5 (2018).
[6]S. Manteghi, A. Sarwar, Z. Fawaz *et al.*, "Mechanical characterization of the static and fatigue compressive properties of a new glass/flax/epoxy composite material using digital image correlation, thermographic stress analysis, and conventional mechanical testing," Mater. Sci. Eng. **99**, 940–950 (2019).
[7]S. S. Pawar and K. Peters, "Through-the-thickness identification of impact damage in composite laminates through pulsed phase thermography," Meas. Sci. Technol. **24**, 115601 (2013).
[8]P. J. Schilling, B. P. R. Karedla, A. K. Tatiparthi *et al.*, "X-ray computed microtomography of internal damage in fiber reinforced polymer matrix composites," Compos. Sci. Technol. **65**(14), 2071–2078 (2005).
[9]S. C. Her and Y. C. Lin, "Assessment of adhesive bond strength using the ultrasonic technique," J. Adhes. **90**(5–6), 545–554 (2014).
[10]N. Mori, N. Matsuda, and T. Kusaka, "Effect of interfacial adhesion on the ultrasonic interaction with adhesive joints: A theoretical study using spring-type interfaces," J. Acoust. Soc. Am. **145(6)**, 3541–3550 (2019).
[11]D. Chicot, P. Araujo, N. Horny *et al.*, "Application of the interfacial indentation test for adhesion toughness determination," Surf. Coat. Technol. **200**(1–4), 174–177 (2005).
[12]A. I. Lavrentyev and J. T. Beals, "Ultrasonic measurement of the diffusion bond strength," Ultrasonics **38**(1–8), 513–516 (2000).

[13]E. Escobar-Ruiz, P. Cawley, P. B. Nagy *et al.*, "Ultrasonic NDE of titanium diffusion bonds using signal phase," Annu. Rev. Prog. Quant. Nondestr. Eval. **32**, 1409–1416 (2013).
[14]E. Escobar-Ruiz, D. C. Wright, P. Cawley *et al.*, "Reflection phase measurements for ultrasonic NDE of titanium diffusion bonds," J. Nondestr. Eval. **33**, 535–546 (2014).
[15]A. I. Lavrentyev and S. I. Rokhlin, "Ultrasonic spectroscopy of imperfect interfaces between a layer and two solids," J. Acoust. Soc. Am. **103**(2), 657–664 (1998).
[16]A. Baltazar, S. I. Rokhlin, and C. Pecorari, "On the relationship between ultrasonic and micromechanical properties of contacting rough surfaces," J. Mech. Phys. Solids **50**(7), 1397–1416 (2002).
[17]T. Z. Qi, L. Lin, S. N. Zhang *et al.*, "Identification interface stiffness of coating/substrate structure based on ultrasonic pressure reflection coefficient amplitude spectrum," Appl. Acoust. **201**, 1–9 (2022).
[18]H. A. Haldren, D. F. Perey, W. T. Yost *et al.*, "Swept-frequency ultrasonic phase evaluation of adhesive bonding in tri-layer structures," J. Acoust. Soc. Am. **145**(3), 1609–1618 (2019).
[19]H. A. Haldren, D. F. Perey, W. T. Yost *et al.*, "A digital, constant-frequency pulsed phase-locked-loop instrument for real-time, absolute ultrasonic phase measurements," Rev. Sci. Instrum. **89**(5), 054902 (2018).
[20]Z. Y. Ma, W. Zhang, Z. B. Luo *et al.*, "Thickness determination of dual-layer coatings based on ultrasonic spectral filtering," Insight: Non-Dest. Test. Cond. Monit. **60**(4), 200–206 (2018).
[21]K. Kendall and D. Tabor, "An ultrasonic study of the area of contact between stationary and sliding surfaces," Proc. R. Soc. Lond. A **323**, 321–340 (1971).
[22]H. G. Tattersall, "The ultrasonic pulse-echo technique as applied to adhesion testing," J. Appl. Phys. **6**(2), 819–832 (1973).
[23]A. I. Lavrentyev and S. I. Rokhlin, "An ultrasonic method for determination of elastic moduli, density, attenuation and thickness of a polymer coating on a stiff plate," Ultrasonics **39**(3), 211–221 (2001).
[24]Z. Y. Ma, Y. Zhao, Z. B. Luo *et al.*, "Ultrasonic characterization of thermally grown oxide in thermal barrier coating by reflection coefficient amplitude spectrum," Ultrasonics **54**(4), 1005–1009 (2014).
[25]Z. Y. Ma, L. M. Sun, Z. B. Luo *et al.*, "Ultrasonic inverse identification of surface integrity of aviation functional coatings through material-oriented regularization," NDT E Int. **133** 102733 (2023).
[26]Z. Y. Ma, Z. B. Luo, L. Lin *et al.*, "Quantitative characterization of the interfacial roughness and thickness of inhomogeneous coatings based on ultrasonic reflection coefficient phase spectrum," NDT E Int. **102**(3), 16–25 (2019).